



ISSN: 0067-2904

Convective heat transfer of Cu – Al₂O₃/water hybrid nanofluid flow in a cavity having vertical wavy sides

Khamis Al Kalbani ^{1*}, M. J. Uddin ²

¹ Faculty of Education and Arts, Sohar University, Sohar, Sultanate of Oman

² Department of Process Engineering, International Maritime College, National University of Science and Technology, Sohar, Sultanate of Oman

Received: 10/6/2023

Accepted: 13/10/2023

Published: 28/2/2025

Abstract

Future hydraulic thermal substances made of hybrid nanofluids have a lot of potentials to fulfill the strict applied thermal energy management specifications of cutting-edge heat flux tricks. Due to synergistic thermal effects and general hydrothermal characteristics, it is necessary to examine the enhanced heat-transfer properties of nanofluids based on hybrid nanomaterials in various advances for the thermal management of machines with advanced heat flux. In a variety of corrugated casings filled with water and a Cu – Al₂O₃/water hybrid nanofluid, the effects of a horizontal magnetic field on natural convection heat transfer have been studied. Finite element techniques (FEM) have been employed to solve the generated dimensionless partial differential equations of the imposed nanofluids. On three distinct wave-shaped heated walls, the streamlines, heat flow, and average Nusselt number for the base fluid and the hybrid nanofluids were plotted and examined. The outcome demonstrates how the device's undulating walls and magnetic field strength have a major impact on heat transfer and heat flow.

Keywords heat transfer, convection, hybrid nanofluids, wavy side, magnetic field

انتقال الحرارة الحملية لتدفق المائع النانوي الهجين ماء/Cu-Al₂O₃ في حاوية بجوانب رأسية مموجة

خاميس بن سيف بن راشد الكلباني^{1*}, محمد جشيم الدين²

¹ كلية التربية والآداب، جامعة صحار، صحار، سلطنة عمان

² قسم هندسة العمليات، كلية عمان البحرية الدولية، الجامعة الوطنية للعلوم والتكنولوجيا، صحار، سلطنة عمان

الخلاصة

تمتلك المواد الحرارية الهيدروليكية المستقبلية المصنوعة من الموائع النانوية الهجينة الكثير من الإمكانيات لتحقيق تطبيقات لإدارة الطاقة الحرارية بمواصفات عالية. نظرًا للتأثيرات الحرارية والخصائص الحرارية المائية العامة، من الضروري فحص خصائص نقل الحرارة المعززة للسوائل النانوية بناءً على المواد النانوية الهجينة في مختلف الأنظمة الحرارية للألات ذات التدفق الحراري المتقدم. في مجموعة متنوعة من الحاويات المموجة المملوءة بالمائع الهجين ماء/Cu-Al₂O₃ تمت دراسة تأثيرات المجال المغناطيسي الأفقي على انتقال الحرارة

*Email: kkalbani@su.edu.om

بالحمل الطبيعي. تم استخدام طريقة العناصر المحدودة (FEM) لحل المعادلات التفاضلية الجزئية عديمة الأبعاد الناتجة عن السوائل النانوية. تم رسم وفحص الخطوط الانسيابية والتدفق الحراري ومتوسط عدد نسلت للسائل الأساسي والسوائل النانوية الهجينة على ثلاثة جدران ساخنة مموجة. أظهرت النتائج مدى تأثير تموج الجدران وقوة المجال المغناطيسي على تدفق الحرارة ومعدل انتقالها.

1. Introduction

A new class of nanosized solid-liquid suspension, known as hybrid nanofluids, holds two or more distinctly separate types of nanoparticles. These types of nanofluids have recently attracted great interest from researchers [1]-[4]. It is a worthy candidate for heat transfer industrial use such as devices that transfer heat from one liquid to another without allowing them to mix, solar panels, thermal tanks, electronic components, biomedical devices, nuclear reactors, oil vehicles, transformers and others. The free heat transfer in a square-shaped device along with a light conductive layer and a solid block was reported by Ghalambaz et al. [5]. Their study looked at Ag-MgO/water hybrid nanofluid and reported that Ag-MgO/water hybrid nanofluid exhibits significantly higher advanced heat transfer than the conventional liquid under consideration. The underlying equations are built using the finite element method and then solved with it. As a result, it was discovered that adding hybrid nanoparticles at a lower Rayleigh number increased the average Nusselt number. However, the heat transfer coefficient reduced with increasing Rayleigh number in the presence of a conductive thermal wall. In a square region with two crumpled flat walls and a hydromagnetic force, Uddin et al. [6] studied the convection of a single component of a copper oxide-water nanofluidic flow to use a semi-kinematic approach. The data show that the average heat transfer increased by 158% when the Rayleigh number increased from 10^4 to 10^6 . The mean heat transfer increased by 11.82% when the volume segment of the nanoparticles was increased from 0.025 to 0.05. The heat transfer rate is higher on the vertical surface of the domains without corrugations. Heat transfer decreases by 16.98% when the wavenumber is increased to 2 and increases by 3.62% when the wavenumber is increased to 4. In a square enclosure with a moving wall saturated with a porous medium and a hot internal obstruction, Jakeer et al. [7] studied magneto-hybrid nanofluidic flow numerically using the finite volume technique. Their investigation proposed using the Cattaneo-Christov heat flow condition to modify the study's mathematical model. According to this, the ratio of convection and conduction declines with rising magnetic field concentration, and the wider the obstacle, the more heat is transferred in a clockwise direction.

Due to its numerous industrial and technical applications, natural convection within a corrugated enclosure has recently received a great deal of attention [8]-[10]. Examples of these enclosures are electrical machines, solar panels and electronic circuit cooling. The effects of geometric and physical properties on hybrid nanofluidic flow and convection inside the cavity with undulating surfaces were reported by Alsabery et al. [11]. They found that copper-alumina-water nanofluids exhibit higher heat transfer after examining and noting the similarities or differences between pure water and other common nanofluids. In a sinusoidal case of heated side faces and a domain filled with three different types of Al_2O_3 nanofluid, pure water, Al_2O_3 -Cu/water hybrid nanofluid and a bottom wall with an isolated heat source, Takabi and Salehi [12] reported a comparative study. They discovered that hybrid nanofluids outperform single-component nanofluids in terms of heat transport. In a cavity with an undulating wall and a hybrid Al_2O_3 -Cu/water nanofluid, Ali [13] numerically examined magnetohydrodynamic pure heat transfer by convection and fluid flow. They also considered a heat-generating cylinder at the domain. The research demonstrated that increasing the buoyancy number could significantly increase fluid motion and heat transfer.

According to the literature review, a curly wall septum is rarely used, particularly for hybrid nanofluids. The current work is a pioneering approach to understanding the heat transfer and osmotic pressure-driven flow properties of a hybrid nanofluid in a different corrugated casing as a function of an axial magnetic force. The structural analysis approach was used to assist in resolving the pertinent partial differential equations. The streamlines are used to describe the flow field. Physical significance is used to study and summarize the impact of important factors on temperature profile and velocity distribution. This type of structure can be used to design engineering tools such as energy storage systems, reactor safety mechanisms, heat exchangers, electronic microchips, and solar technologies.

2. Physical Modelling

In the current study, we used nanofluidic flow to analyze time-dependent, incompressible, laminar, and two-dimensional flow. The hydromagnetic and opposing gravitational forces were used to build a nano-fluidic model, where the equation space is a square of length L and filled with a copper-alumina-water two-component hybrid nanofluid. The y -axis is normally next to the left wall and the x -axis measures along the bottom surface in dimensional coordinates. The equations for wavy walls are:

$$\begin{aligned} x_{left} &= A \cos\left(\frac{N\pi y}{L}\right), x_{right} \\ &= A \cos\left(\frac{N\pi y}{L}\right) + L, \end{aligned} \quad (1)$$

where $A = 0.05, N = 0, 4, 8$.

Regarding the coordinate system, a magnetic field with a strength of B_0 is applied. The upper and underside walls are insulated, and the right and left side walls are used to isothermally cool and heat nanofluids at uniform temperatures of T_C and T_H correspondingly. It is always maintained that, $T_H > T_C$. The Cu – Al₂O₃ hybrid nanoparticles and water were used as the base fluid in the current study. Figure 1 illustrates the geometry and coordinates system schematically.

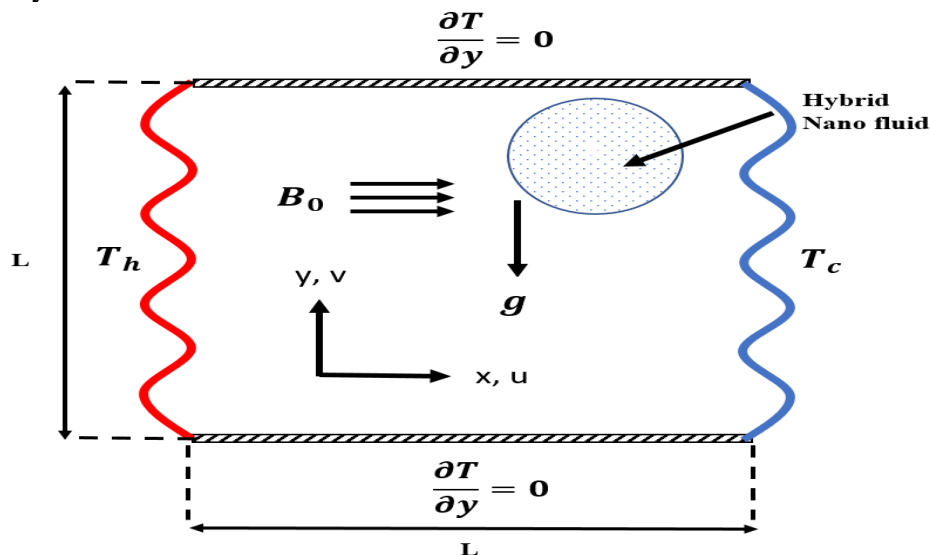


Figure 1: Physical model's schematic view

It is also expected that the reference solution and the nanomaterials are in thermodynamic equilibrium and that there is no slippage between the two media. Despite the density change in the body force element of the momentum equation estimated using the Boussinesq

assumption, the physical properties of the nanofluids were assumed to be static. The acceleration due to gravity has a negative y-direction. Since all fixed boundaries are assumed to be rigid, the walls do not move. Table 1 is a listing of the thermophysical properties of nanofluids.

Table 1: Thermo-physical characteristics of solid nanoparticles and the base fluid (Oztop and Abu-Nada [14]).

Items	Unit	water	Cu	Al ₂ O ₃
c_p	J/kgK	4179	385	765
ρ	kg/m ³	997.1	8933	3970
k	W/mK	0.613	401	40
μ	Ns/m ²	0.001	-	-
σ	s/m	5.5×10^{-6}	59.6×10^6	35×10^6
β	1/K	21×10^{-5}	1.67×10^{-5}	0.85×10^{-5}

3. Mathematical Modelling

Assuming that the flow is continuous and laminar and that the nanofluid is Newtonian, a set of basic equations for nanofluids was modified. The incompressible Navier-Stokes equations were used to model the flow in two dimensions. The density variation was examined using the Boussinesq approximation. Mass, momentum and energy conservation were accounted for using the accompanying mathematical equations. Given the above premises, the governing equations [15] for this model have been conveyed as follows:

$$\frac{\partial u}{\partial x} + \frac{\partial v}{\partial y} = 0, \quad (2)$$

$$u \frac{\partial u}{\partial x} + v \frac{\partial u}{\partial y} = -\frac{1}{\rho_{hnf}} \frac{\partial p}{\partial x} + \frac{\mu_{hnf}}{\rho_{hnf}} \left(\frac{\partial^2 u}{\partial x^2} + \frac{\partial^2 u}{\partial y^2} \right), \quad (3)$$

$$u \frac{\partial v}{\partial x} + v \frac{\partial v}{\partial y} = -\frac{1}{\rho_{hnf}} \frac{\partial p}{\partial y} + \frac{\mu_{hnf}}{\rho_{hnf}} \left(\frac{\partial^2 v}{\partial x^2} + \frac{\partial^2 v}{\partial y^2} \right) + g(T - T_C) \frac{(\rho\beta)_{hnf}}{\rho_{hnf}}, \quad (4)$$

$$u \frac{\partial T}{\partial x} + v \frac{\partial T}{\partial y} = \alpha_{hnf} \left(\frac{\partial^2 T}{\partial x^2} + \frac{\partial^2 T}{\partial y^2} \right) \quad (5)$$

The parameters of the hybrid nanofluid are defined as follows [15-16]:

$$\rho_{hnf} = \rho_{bf} (1 - \varphi_{hnf}) + \rho_{n1} \varphi_{n1} + \rho_{n2} \varphi_{n2} \quad (6)$$

$$(\rho\beta)_{hnf} = (\rho\beta)_{bf} (1 - \varphi_{hnf}) + (\rho\beta)_{n1} \varphi_{n1} + (\rho\beta)_{n2} \varphi_{n2} \quad (7)$$

$$\text{Where } \varphi_{hnf} = \varphi_{n1} + \varphi_{n2}$$

$$\alpha_{hnf} = \frac{k_{hnf}}{(\rho c_p)_{hnf}}, \quad (8)$$

$$(\rho c_p)_{hnf} = (1 - \varphi_{n2}) \left[(1 - \varphi_{n1}) (\rho c_p)_{bf} + \varphi_{n1} (\rho c_p)_{n1} + \varphi_{n2} (\rho c_p)_{n2} \right] \quad (9)$$

$$\mu_{hnf} = \frac{\mu_{bf}}{(1 - \varphi_{n1})^{2.5} (1 - \varphi_{n2})^{2.5}}, \quad (10)$$

$$k_{hnf} = \frac{k_{n2} + 2k_{nf} - 2\varphi_{n2}(k_{nf} - k_{n2})}{k_{n2} + 2k_{nf} + \varphi_{n2}(k_{nf} - k_{n2})} (k_{nf}), \quad (11)$$

$$k_{nf} = \frac{k_{n1} + 2k_{bf} - 2\varphi_{n1}(k_{bf} - k_{n1})}{k_{n1} + 2k_{bf} + \varphi_{n1}(k_{bf} - k_{n1})} (k_{bf}) \quad (12)$$

The following are the different types of boundary conditions for the current investigation:

$$u = v = 0, T = T_H \text{ for } x_{left}; 0 \leq y \leq L$$

(13a)

$$u = v = 0, T = T_C \text{ for } x_{right}; 0 \leq y \leq L \quad (13b)$$

$$u = v = 0, \frac{\partial T}{\partial y} = 0 \text{ for } y = 0, L; 0 \leq x \leq L$$

(13c)

The following transformations can be used to make the aforementioned equations dimensionless:

$$X = \frac{x}{L}, Y = \frac{y}{L}, U = \frac{uL}{\alpha_{bf}}, V = \frac{vL}{\alpha_{bf}}, P = \frac{pL^2}{\rho_{bf}\alpha_{bf}^2},$$

$$\theta = \frac{T - T_C}{T_H - T_C} \quad (14)$$

With equation (14), the governing equations (2) through (5) can be expressed in the dimensionless form as follows:

$$\frac{\partial U}{\partial X} + \frac{\partial V}{\partial Y} = 0, \quad (15)$$

$$\left(\frac{\rho_{hnf}}{\rho_{bf}}\right) \left(U \frac{\partial U}{\partial X} + V \frac{\partial U}{\partial Y} \right) = - \frac{\partial P}{\partial X} + \frac{Pr}{(1-\varphi_{n1})^{2.5} (1-\varphi_{n2})^{2.5}} \left(\frac{\partial^2 U}{\partial X^2} + \frac{\partial^2 U}{\partial Y^2} \right), \quad (16)$$

$$\left(\frac{\rho_{hnf}}{\rho_{bf}}\right) \left(U \frac{\partial V}{\partial X} + V \frac{\partial V}{\partial Y} \right)$$

$$= - \frac{\partial P}{\partial Y} + \frac{Pr}{(1-\varphi_{n1})^{2.5} (1-\varphi_{n2})^{2.5}} \left(\frac{\partial^2 V}{\partial X^2} + \frac{\partial^2 V}{\partial Y^2} \right) + (Ra)(Pr) \frac{(\rho\beta)_{hnf}}{\rho_{bf}\beta_{bf}} \theta$$

$$- Ha^2 Pr V \quad (17)$$

$$U \frac{\partial \theta}{\partial X} + V \frac{\partial \theta}{\partial Y} = \frac{\alpha_{hnf}}{\alpha_{bf}} \left(\frac{\partial^2 \theta}{\partial X^2} + \frac{\partial^2 \theta}{\partial Y^2} \right) \quad (18)$$

Where $Pr = \frac{\nu_{bf}}{\alpha_{bf}}$ is the Prandtl number, $Ra = \frac{g\beta_{bf}(T_H - T_C)L^3}{\alpha_{bf}\nu_{bf}}$ is the Rayleigh number and

$Ha = B_0 L \sqrt{\frac{\sigma_{bf}}{\mu_{bf}}}$ is the Hartmann number.

The boundary conditions' dimensionless forms include:

$$U = V = 0, \theta = 1 \text{ for } X_{left}; 0 \leq Y \leq 1 \quad (19a)$$

$$U = V = 0, \theta = 0 \text{ for } X_{right}; 0 \leq Y \leq 1 \quad (19b)$$

$$U = V = 0, \frac{\partial \theta}{\partial Y} = 0 \text{ for } Y = 0, 1; 0 \leq X \leq 1 \quad (19c)$$

At the heated bottom wall, it is estimated that the local Nusselt number is:

$$Nu_{hnf} = - \left(\frac{k_{hnf}}{k_{bf}} \right) \left(\frac{\partial \theta}{\partial X} \right)_{X=0} \quad (20)$$

Furthermore, the local Nusselt number is integrated to produce the average Nusselt number:

$$\overline{Nu}_{hnf} = \int_0^1 Nu_{hnf} dY \quad (21)$$

4. Numerical Solution and Validation

Various mesh combinations of the geometry were tested to determine the best heat transfer rate and flow fields. During the grid test, the following parameter set combinations were used: $Ra = 10^5$, $\varphi_{n1} = 0.03$, $\varphi_{n2} = 0.03$, $Ha = 20$, $Pr = 6.838$, and $N = 8$. Four different non-standard grid systems were used in the simulation system to assess the expected number of elements for the constrained area. The arithmetic pattern is completed to extremely accurately input in the typical Nusselt number (Nu_{av}) for the elements mentioned above as shown in Table 2 in order to understand the mesh size. We noticed that the average Nusselt number (Nu_{av}) for 5554 elements showed a small difference contrasted with the results for the 7990 elements. Therefore, the grid size of 5554 and 7990 elements can be used to get accurate results, and 7990 triangle elements were considered in the simulation to generate the results.

Table 2: Grid sensitivity test at $Ra = 10^5$, $\varphi_{n1} = 0.03$, $\varphi_{n2} = 0.03$, $Pr = 6.838$, $Ha = 20$ and $N = 8$ for Cu – Al₂O₃/water nanofluid at the left wavy wall of the cavity.

Elements	3440	5554	7990	18120
Nu_{av}	3.023	3.005	3.002	2.989

We compared our results for the predetermined conditions with previously published results by Ghasemi et al. [18]. For this comparison, we selected: $\varphi_{n1} = 0$, $\varphi_{n2} = 0, 0.02, 0.06$, $N = 0$ for calculating the average Nusselt number presented in Table 3. In both studies, the average Nusselt number is calculated at the heated cavity wall for similar buoyancy forces. The current simulation results and the results of Ghasemi et al. [18] agree very closely. The numerical results of the study are now more credible and validated further results.

Table 3: Comparison between the data of Ghasemi et al. (2011) and the present work

Ra	$\varphi = 0$		$\varphi = 0.02$		$\varphi = 0.06$	
	Present	Ghasemi et al. (2011)	Present	Ghasemi et al. (2011)	Present	Ghasemi et al. (2011)
10^3	1.002	1.001	1.060	1.160	1.184	1.184
10^4	1.182	1.179	1.224	1.302	1.319	1.291
10^5	3.137	3.151	3.180	3.138	3.259	3.108
10^6	7.81	7.907	7.957	7.979	8.223	8.098

5. Results and Discussion

This section examines the effects of the ripple parameter N on the streamlines and local heat flux and the average Nusselt number at the heated wall for both the pure fluid and the hybrid nanofluid. The results were obtained for different values of the Rayleigh number and Hartmann's number. The results are presented and analyzed from a physical and technical point of view. The Rayleigh number ranges from 10^4 to 10^6 while the ripple parameter ranges from 0 to 8. These are the variations in the physical properties of the problem. Initially, it is observed that the heat transfer and the velocity distributions for various nanofluids and base fluids are similar in the cavity even with various wave numbers for the lower buoyancy forces and the opposite pictures can be observed in the higher buoyancy forces.

Figure 2 is a hybrid nanofluid flow field visualization (Streamlines) for different values of Rayleigh number (Ra) and different values of N when $\varphi_{n1} = 0.02$, $\varphi_{n2} = 0.03$, $Ha = 0$, $Pr = 6.838$. The flow structure depicts a clockwise circulation and a high vorticity field upwards near the vertical walls due to a higher buoyancy force as the Rayleigh number increases. However, as the undulation parameter N increases, the vorticity weakens due to the conduction transfer dominant.

When the magnetic field is considered in Figure 3 with $Ha = 30$, a weaker clockwise circulation in the cavity is observed. The magnetic field aligns the fluid flow along its lines of force. Nearby the wavy side, the alignment could mitigate the swirling motion, resulting in a weaker clockwise circulation compared to the scenario without a magnetic field. Furthermore, the orientation of the magnetic field concerning the wavy enclosure geometry can affect how the Lorentz force interacts with the fluid flow, potentially altering circulation patterns. Moreover, the irregularities in the wavy enclosure might interact differently with the magnetic field, leading to variations in the flow behavior and circulation patterns.

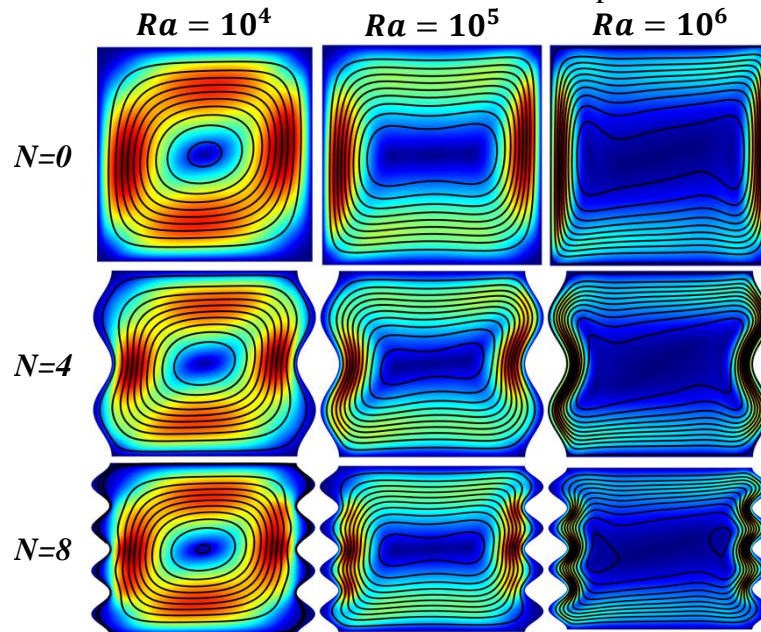


Figure 2: Streamlines for the Rayleigh number (Ra) and N for without magnetic effect $Ha = 0$ when $\varphi_{n1} = 0.02$, $\varphi_{n2} = 0.03$, $Pr = 6.838$.

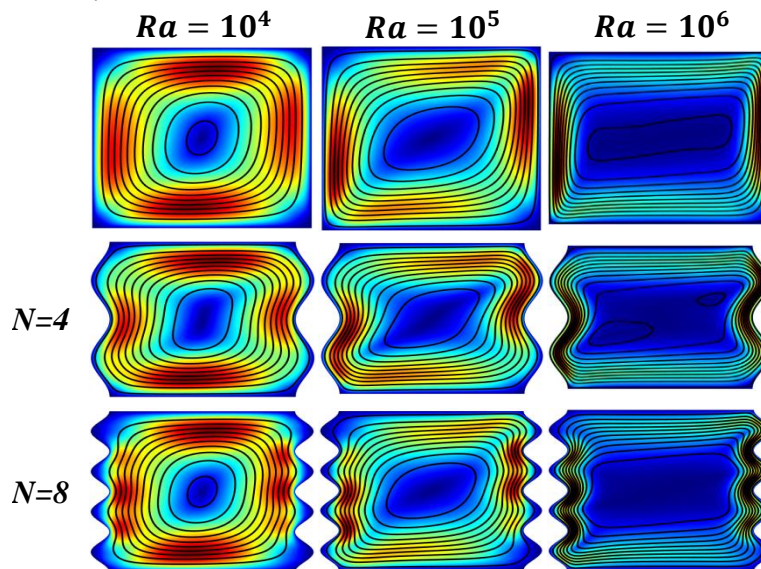


Figure 3: Streamlines for Rayleigh number (Ra) and N for the presence of $Ha = 30$, when $\varphi_{n1} = 0.02$, $\varphi_{n2} = 0.03$, $Pr = 6.838$.

Figures 4-6 display the total heat flux on the heated wall of the field. The findings described triplet values of the Rayleigh numbers ($Ra = 10^4, 10^5, 10^6$) with three values of the undulation parameter N ($N = 0, 4, 8$). The findings show that the strengthened buoyant flow increases the heat transfer rate as the Rayleigh number increases in all three cases. This

is because increasing Rayleigh number boosts buoyancy-driven convection, accelerating fluid movement and heat transfer within the enclosure, facilitated by enhanced nanofluid thermal properties and improved mixing due to the intensified buoyancy effects. Moreover, as the parameter N increases, the heat transfer increases by fostering complex flow patterns, intensifying turbulence-induced mixing. Increasing surface area for heat exchange, and promoting better fluid-wall interaction, could collectively contribute to heightened heat transfer rates within the enclosure. In Figure 4, it is noticeable that for $Ra = 10^4$ the heat transfer shows a horizontal line since the conduction regime dominated. Then as Ra increases, the heat transfer shows an increase and then a decrease. This is due to the convection-dominated regime. In Figures 5 and 6, even though the heat transfer is high, the graph lines take the shape of the wavy side with a slight difference. This is because the wavy shape side delays the convection regime.

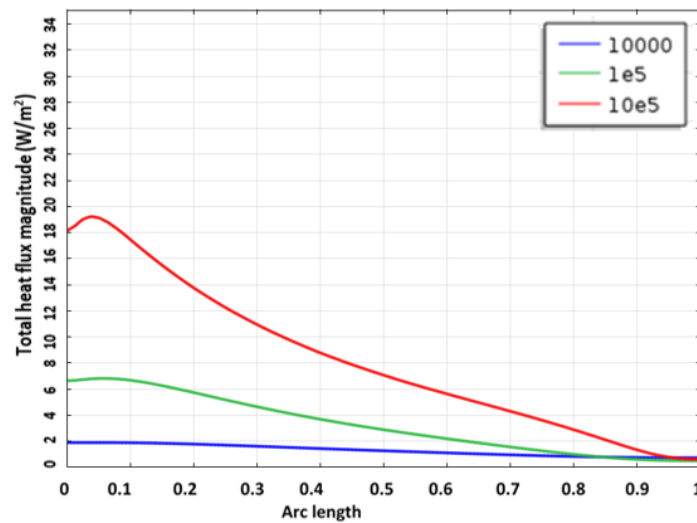


Figure 4: Total heat flux magnitude for Rayleigh number (Ra) for $N = 0$, $\varphi_{n1} = 0.02$, $\varphi_{n2} = 0.03$, $Ha = 30$, $Pr = 6.838$.

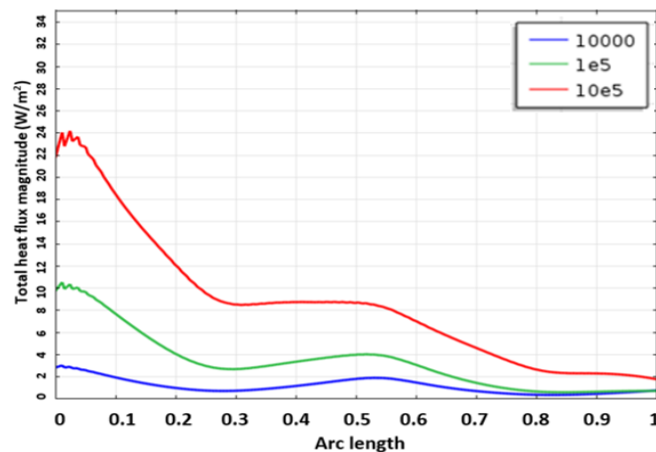


Figure 5: Total heat flux magnitude for different values of Rayleigh number (Ra) for $N = 4$, $\varphi_{n1} = 0.02$, $\varphi_{n2} = 0.03$, $Ha = 30$, $Pr = 6.838$.

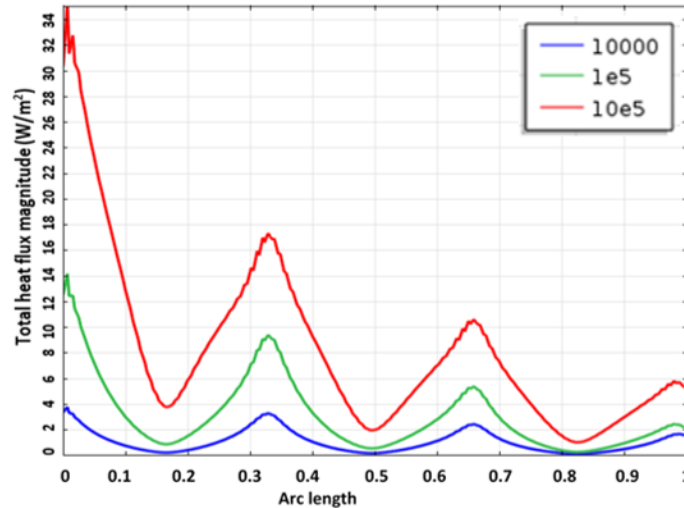


Figure 6: Total heat flux magnitude for Rayleigh number (Ra) for $N = 8$, $\varphi_{n1} = 0.02$, $\varphi_{n2} = 0.03$, $Ha = 30$, $Pr = 6.838$.

An average Nusselt number is calculated on the heated wall and displayed in Figure 7 for water base fluid with no magnetic field effect for different Rayleigh numbers and undulation parameter N . The lines for $N = 0$ and $N = 4$ almost coincide, but the average Nusselt number line dropped significantly when $N = 8$. This indicates that the convection regime is delayed as N increases while the conduction heat transfer prevails. By adding $Cu - Al_2O_3$ hybrid nanoparticles ($\varphi_{n1} = 0.02, \varphi_{n2} = 0.03$) to the water, the average Nusselt number is increased for all three cases of N , as illustrated in Figure 8. This is due to the high thermal conductivity of Copper and Aluminum oxide and a reduced thermal resistance at the fluid-wall interfaces. We also noticed that the average Nusselt number calculation for the base fluid water is significantly higher, almost 18%, than that of the hybrid nanofluid studied.

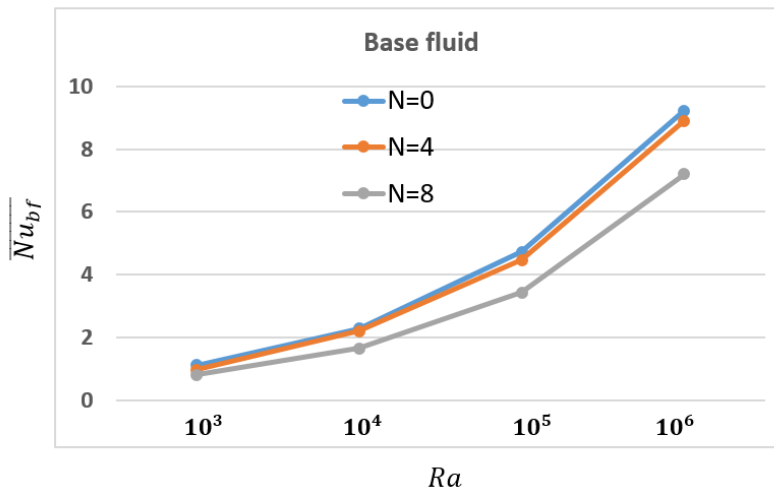


Figure 7: Average Nusselt number for Rayleigh number (Ra) and N for base fluid when $\varphi_{n1} = 0$, $\varphi_{n2} = 0$, $Ha = 0$, $Pr = 6.838$.

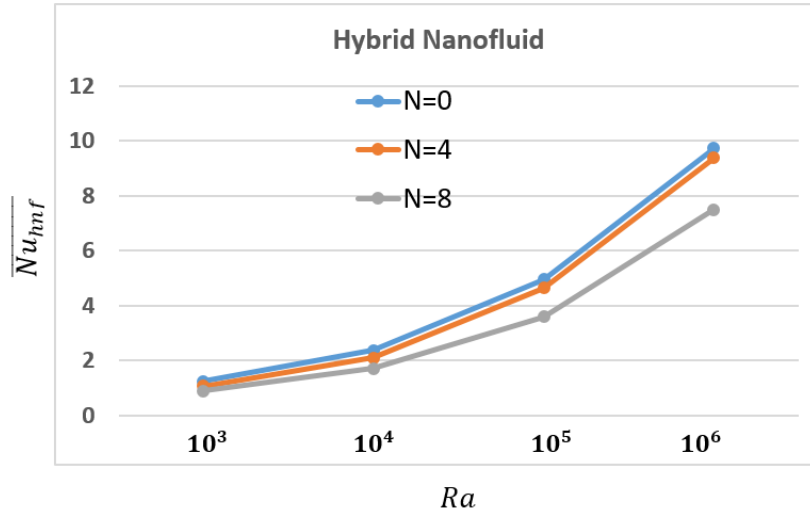


Figure 8: Average Nusselt number for Rayleigh number (Ra) and N for hybrid nanofluid when $\varphi_{n1} = 0.02$, $\varphi_{n2} = 0.03$, $Ha = 0$, $Pr = 6.838$.

The average Nusselt number for pure water and hybrid nanofluid under the effect of the magnetic field is shown in Figures 9 and 10, respectively. With an intensifying magnetic field, it is apparent that the average Nusselt number falls. An increasing horizontal magnetic field disrupts fluid flow patterns, including resistance via eddy currents, impeding convective heat transfer within the enclosure, consequently decreasing the overall heat transfer rate. Particularly significant is the fact that with increased buoyancy, the average Nusselt number for heat transmission grows exponentially. The average Nusselt number at the higher levels of the Rayleigh number is around 27% larger when the ripple parameter is $N = 4$ rather than $N = 8$.

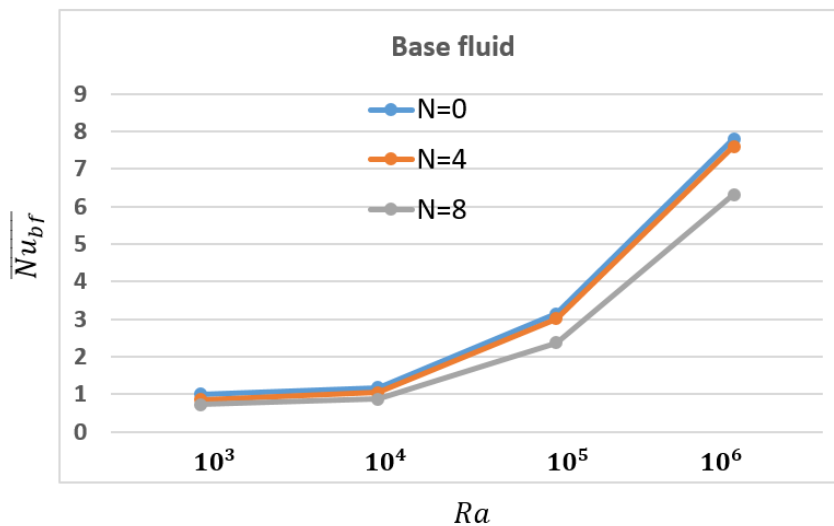


Figure 9: Average Nusselt number for Rayleigh number (Ra) and N for base fluid when $\varphi_{n1} = 0$, $\varphi_{n2} = 0$, $Ha = 30$, $Pr = 6.838$.

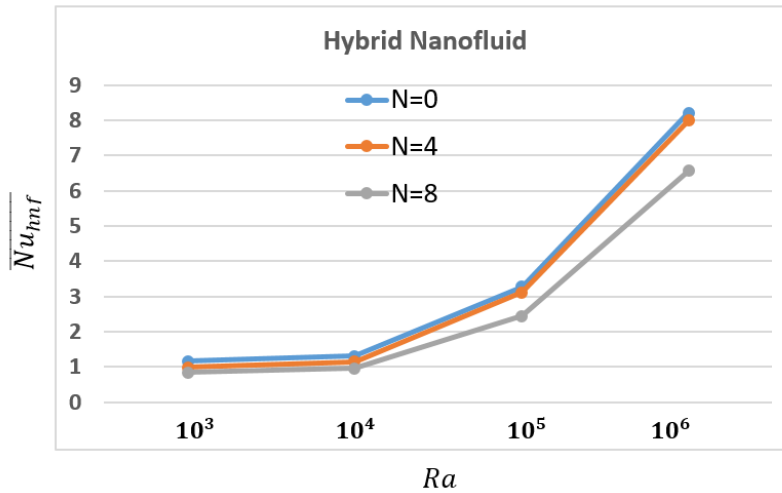


Figure 10: Average Nusselt number for Rayleigh number (Ra) and N for hybrid nanofluid when $\varphi_{n1} = 0.02$, $\varphi_{n2} = 0.03$, $Ha = 30$, $Pr = 6.838$.

Table 4: Average Nusselt number for different values of N and different fractions of φ_{n1} , φ_{n2} when $Ra = 10^5$, $\varphi = 0.05$, $Ha = 30$, $Pr = 6.838$.

N	φ_{n1}	φ_{n2}										
	0	0.05	0.01	0.04	0.02	0.03	0.03	0.02	0.04	0.01	0.05	0
0	3.241		3.255		3.268		3.279		3.29		3.3	
4	3.08		3.1		3.111		3.122		3.133		3.142	
8	2.429		2.439		2.449		2.458		2.467		2.474	

The average Nusselt number for Normal and hybrid nanofluid was measured at different fractions of Cu – Al_2O_3 nanoparticle concentration and three different undulation parameter values ($N = 0, 4, 8$) with $Ra = 10^5$, $\varphi = 0.03$ and $Ha = 30$. Results in Table 4 showed that as the fraction of Cu nanoparticles increases, the average Nusselt number increases for all three cases. This is attributed to the higher thermal conductivity of Cu nanoparticles compared to that of Al_2O_3 nanoparticles. The highest Nusselt number was found when the undulation parameter N was set to 0, the Cu nanoparticle concentration was 0.05, and the Al_2O_3 concentration was 0. These findings suggest that using a Cu – water nanofluid is a better option for thermal performance when compared by Cu – Al_2O_3 /water hybrid nanofluid.

6. Conclusion

Heat transfer and flow were analyzed in a cavity with vertical wavy walls to understand the effects of relevant parameters such as Hartmann number (magnetic field number), Rayleigh number and undulation parameter of the vertical walls. The most important simulation results can be summarized as follows:

- With the escalation of the Rayleigh number, buoyancy amplifies, resulting in a clockwise flow and heightened vorticity proximal to the vertical walls.
- The heat flux at the heated wall varies slightly between the ripple parameters $N = 0$ and $N = 4$ but falls off, when $N = 8$.
- Increasing the ripple parameter N , the total heat flux at the heated wall increases. However, the average Nusselt number decreases for both hybrid nanofluid and base fluid.

- The hybrid nanofluid improves the heat transfer rate compared to the base fluid.
- The rate of heat transfer decreases as the horizontal magnetic field increases.
- Due to the small circulations and the thermal boundary layer on the wavy heated wall, the wavy side delays the convection regime.
- Cu – water nanofluid shows better performance in heat transfer rate when compared to Cu – Al₂O₃/water hybrid nanofluid.

References

- [1] M. M. Rashidi, M. Sadri, M. A. Sheremet, "Numerical simulation of hybrid nanofluid mixed convection in a lid-driven square cavity with magnetic field using high-order compact scheme." *Nanomaterials*, vol.11, no. 2250, pp. 2250, 2021.
- [2] M. Abed, A. Aissa, F. Mebarek-Oudina, W. Jamshed, W. Ahmed, H. M. Ali, A. M. Rashad, A. M. "Galerkin finite element analysis of thermal aspects of Fe₃O₄-MWCNT/water hybrid nanofluid filled in wavy enclosure with uniform magnetic field effect." *International Communications in Heat and Mass Transfer*, vol. 126, no. 105461, pp. 105461, 2021.
- [3] C. Revnic, T. Groşan, M. Sheremet, I.Pop, "Numerical simulation of MHD natural convection flow in a wavy cavity filled by a hybrid Cu-Al₂O₃-water nanofluid with discrete heating". *Applied Mathematics and Mechanics*, vol.41, pp. 1345-1358, 2020.
- [4] B. A. I. Bendrer, A. Abderrahmane, S. E. Ahmed, Z. A. Raizah, "3D magnetic buoyancy-driven flow of hybrid nanofluids confined wavy cubic enclosures including multi-layers and heated obstacle" *International Communications in Heat and Mass Transfer*, vol. 126, pp 105431.2021.
- [5] M. Ghalambaz, A. Doostani, E. Izadpanahi, A. j. Chamkha, "Conjugate natural convection flow of Ag–MgO/water hybrid nanofluid in a square cavity" *Journal of Thermal Analysis and Calorimetry*, vol. 139, pp. 2321-2336. 2020.
- [6] M. j. Uddin, S. K. Rasel, J. K. Adewole, and K.S. Al Kalbani, "Finite element simulation on the convective double diffusive water-based copper oxide nanofluid flow in a square cavity having vertical wavy surfaces in presence of hydro-magnetic field". *Results in Engineering*, vol.13, pp 100364, 2022.
- [7] S. Jakeer, P. B. Reddy, A. M. Rashad, H. A. Nabwey, "Impact of heated obstacle position on magneto-hybrid nanofluid flow in a lid-driven porous cavity with Cattaneo-Christov heat flux pattern" *Alexandria Engineering Journal*, vol. 60, no.1, pp. 821-835,2021.
- [8] K. Kalyani, S. Rani MVVNL. "A numerical study on cross diffusion cattaneo-christov impacts of MHD micropolar fluid across a paraboloid." *Iraqi Journal of Science* pp. 1238-1264.2021.
- [9] G. K. Narender, Govardhan, G. Sreedhar Sarma. "Numerical study of radiative magnetohydrodynamics viscous nanofluid due to convective stretching sheet with the chemical reaction effect" *Iraqi Journal of Science*, vol. 61, no. 7, pp. 1733-1744. 2020.
- [10] K. W. Sadiq, D. G. S. Al-Khafajy. "Influence of heat transfer on Magneto hydrodynamics oscillatory flow for Williamson fluid through a porous medium." *Iraqi Journal of Science* , vol. 59, no. 1B , pp. 389-397, 2020.
- [11] Alsabery, A. I., Tayebi, T., Kadhim, H. T., Ghalambaz, M., Hashim, I., & Chamkha, A. J. "Impact of two-phase hybrid nanofluid approach on mixed convection inside wavy lid-driven cavity having localized solid block." *Journal of Advanced Research*, vol. 30, pp. 63-74,2021.
- [12] T. Behrouz, S. Salehi. "Augmentation of the heat transfer performance of a sinusoidal corrugated enclosure by employing hybrid nanofluid." *Advances in Mechanical Engineering*, vol. 6, pp. 147059, 2014.
- [13] A. M. Mokaddes, R. Akhter, M. A. Alim. "Hydromagnetic natural convection in a wavy-walled enclosure equipped with hybrid nanofluid and heat generating cylinder." *Alexandria Engineering Journal*, vol. 60, no.6, pp. 5245-5264, 2021
- [14] Oztop, F. Hakan E. Abu-Nada. "Numerical study of natural convection in partially heated rectangular enclosures filled with nanofluids." *International Journal of Heat and Fluid Flow*, vol. 29, no.5, pp. 1326-1336, 2008.

- [15] Lai, F. H., and Yang, Y. T. Lattice Boltzmann simulation of natural convection heat transfer of Al₂O₃/water nanofluids in a square enclosure. *International Journal of Thermal Sciences*, vol.50, no.10, pp.1930-1941, 2011
- [16] Nasrin, Rehana, and M. A. Alim. "Free convective flow of nanofluid having two nanoparticles inside a complicated cavity." *International Journal of Heat and Mass Transfer*, vol. 63, pp.191-198., 2013.
- [17] J. Raza, A. M. Rohni, Z. Omar, Numerical investigation of copper-water (Cu-water) nanofluid with different shapes of nanoparticles in a channel with stretching wall: slip effects. *Mathematical and Computational Applications*, vol.21, no.4, pp.43, 2016.
- [18] B. Ghasemi, S. M. Aminossadati, A. Raisi. "Magnetic field effect on natural convection in a nanofluid-filled square enclosure." *International Journal of Thermal Sciences*, vol. 50, no.9, pp. 1748-1756, 2016.

Nomenclature

A	amplitude [m]
B_0	magnetic field strength [kg/s ² . A]
c_p	specific heat at constant pressure [J/kgK]
g	gravitational acceleration [m/s ²]
Ha	Hartmann number [-]
k	thermal conductivity [W/mK]
L	enclosure length [m]
N	undulation parameter [m]
Nu	Nusselt number [-]
p	dimensional fluid pressure [Pa]
p	dimensionless fluid pressure [-]
Pr	Prandtl number [-]
Ra	Rayleigh number [-]
T	Temperature [K]
u, v	dimensional velocity components [m/s]
U, V	dimensionless velocity components [-]
x, y	dimensional coordinates [m]
X, Y	dimensionless coordinates [-]

Greek symbols

α	thermal diffusivity [m ² /s]
β	thermal expansion coefficient [1/K]
θ	dimensionless temperature [-]
μ	dynamic viscosity [Ns/m ²]
ν	kinematic viscosity [m ² /s]
ρ	density [kg/m ³]
σ	electrical conductivity [S/m]
φ	nanoparticle volume fraction [-]

Subscript

av	average
bf	base fluid
C	cold wall
H	hot wall
hnf	hybrid nanofluid
$n1$	copper nanoparticle
$n2$	aluminum oxide nanoparticle
nf	nanofluid